Material Properties and Operating Configurations of Membrane Reactors for Propane Dehydrogenation

Seung-Won Choi, Christopher W. Jones, Sankar Nair, and David S. Sholl
School of Chemical & Biomolecular Engineering, Georgia Institute of Technology, Atlanta, GA 30332

Jason S. Moore, Yujun Liu, Ravindra S. Dixit, and John G. Pendergast
Engineering & Process Sciences, The Dow Chemical Company, Freeport, TX 77541

DOI 10.1002/aic.14700
Published online December 11, 2014 in Wiley Online Library (wileyonlinelibrary.com)

A modeling-based approach is presented to understand physically realistic and technologically interesting material properties and operating configurations of packed-bed membrane reactors (PBMRs) for propane dehydrogenation (PDH). PBMRs composed of microporous or mesoporous membranes combined with a PDH catalyst are considered. The influence of reaction and membrane transport parameters, as well as operating parameters such as sweep flow and catalyst placement, are investigated to determine desired "operating windows" for isothermal and nonisothermal operation. Higher Damköhler (Da) and lower Péclet (Pe) numbers are generally helpful, but are much more beneficial with highly H_2-selective membranes rather than higher-flux, lower-selectivity membranes. H_2-selective membranes show a plateau region of conversion that can be overcome by a large sweep flow or countercurrent operation. The latter shows a complex trade-off between kinetics and permeation, and is effective only in a limited window. H_2-selective PBMRs will greatly benefit from the fabrication of thin (∼1 μm or less) membranes. © 2014 American Institute of Chemical Engineers *AIChE J*, 61: 922–935, 2015

Keywords: membrane reactor, propane dehydrogenation, zeolite membrane, modeling, propane dehydrogenation catalyst

Introduction

Propylene is an important petrochemical feedstock for production of polypropylene and other chemical products. Propylene can be produced from steam cracking or by propane dehydrogenation (PDH).[1–5] PDH is especially attractive in North America and the Middle East, where there is an abundant supply of propane. However, the conversion in PDH is thermodynamically limited, and it is energy intensive because of its highly endothermic nature. Furthermore, the downstream separation of propylene from its equilibrium mixture with propane is also energy intensive because of the small relative volatility between the two. The separation is currently accomplished in cryogenic distillation columns with more than 100 trays.[6] One way to overcome the equilibrium limitations of reactions like PDH is to intensify them via membrane reactors.[7–9] Among different possible membrane reactor configurations, the packed bed membrane reactor (PBMR) consists of a membrane surrounding a conventional tubular packed bed reactor (PBR). The permselective membrane permeates one or more of the reaction products, thus shifting the equilibrium to the product side. This enhances the productivity of PDH and also reduces the cost of the downstream separation.

The applications of PBMRs have been studied for different reactions with various types of membranes. In early studies, Ziaka et al. reported enhanced conversion and selectivity for PDH using a membrane reactor with commercial ceramic membranes.[10,11] Collins et al. also observed moderate improvements in PDH performance using hydrogen-selective palladium and silica membranes.[12] Recently, Kong et al. used pure-silica MFI zeolite membranes for dehydrogenation of ethyl benzene and investigated the effect of sweep gas on conversion enhancement.[13] Kim et al. studied membrane reactors based on MFI zeolite membranes for the water-gas shift reaction and observed enhanced CO conversion.[14] In addition to experimental work, mathematical modeling of PBMRs has also been performed. Wu and Liu built a model for dehydrogenation of ethyl benzene using a ceramic membrane with performance based on Knudsen diffusion.[15] Kumar et al. studied a membrane reactor for dehydrogenation of cyclohexane using FAU zeolite membranes, for which the permeances were described by empirical equations as a function of temperature.[16] Van den Bergh et al. also investigated isobutene dehydrogenation in a DDR zeolite membrane reactor with both modeling and experimental approaches.[17] The relationship between membrane permeation and kinetic reaction rates has been suggested by Harold et al., who reported an optimal range of membrane permeation rates for different membrane selectivities to achieve

Additional Supporting Information may be found in the online version of this article.

Correspondence concerning this article should be addressed to S. Nair at sankar.nair@chbe.gatech or D. S. Sholl at david.sholl@chbe.gatech.edu.

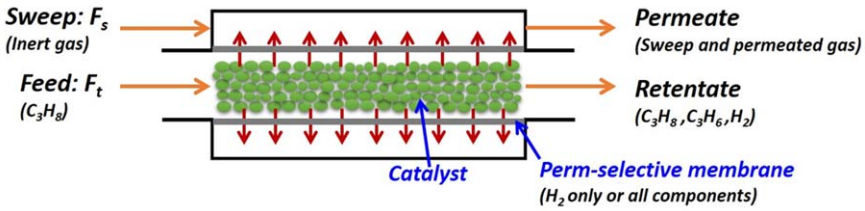

Figure 1. Schematic of a PDH PBMR.

The red arrows denote flux through the membrane surrounding the packed bed. [Color figure can be viewed in the online issue, which is available at wileyonlinelibrary.com.]

maximum conversion in cyclohexane dehydrogenation.[18] Gokhale et al. have used dimensional analysis to study the effects of residence time and membrane selectivity for isobutane dehydrogenation.[19] More detailed two-dimensional (2-D) models and nonisothermal models have also been developed. Tsai et al. carried out nonisothermal modeling for partial oxidation of methane and studied temperature profiles in adiabatic operating conditions.[20] Shelepova et al. developed a model of combined oxidation of hydrogen (exothermic) in the shell side with PDH (endothermic) in the tube.[21] Modeling of countercurrent sweep gas configuration has also been studied and compared with cocurrent mode by several research groups.[22–24]

The above studies show clear potential for obtaining enhancement in conversion over conventional reactors. Although complex models for membrane reactors have been developed, the previous works have considered the PBMR performance (e.g., conversion and yield) only in a limited range of operating conditions and material parameters. Relatively little attention has so far been paid to understanding in detail the operating "windows" of PBMRs as a function of the catalyst and membrane performance parameters and the system operating parameters, particularly for PDH. Such a study would be useful in the design and selection of appropriate PDH PBMR materials and configurations for target applications, and in understanding the complex interaction of membrane permeation and catalyst kinetics in PBMRs. In the present study, we first construct a sufficiently detailed model of PDH in a PBMR and then use it to systematically study the PBMR performance characteristics over a wide range of possible material and operating parameters, including cocurrent and countercurrent sweep modes. For the sake of simplicity, our model does not consider nonisothermal operation or radial dispersion. Our approach here is to use a relatively simple model to identify appropriate operating windows for PDH PBMRs, which can then be investigated in further detail via more complex models and targeted experiments. We use dimensional analysis to identify the operating windows for PDH PBMRs for desired performance levels and to specify realistic yet high-performance membranes, catalysts, and operating configurations. Building upon previous PBMR modeling literature for other dehydrogenation reactions,[18,19,25] we present here a more detailed investigation of PDH PBMRs covering a broad range of material and operating parameters, operating configurations such as counter current sweep gas operation and multiple membrane tubes, and place greater emphasis on determining the required membrane properties necessary to obtain target performance in the PDH reaction. Another objective of this work is to better understand the interaction of mass transport and reaction kinetics in the operating windows and to clarify the realistic upper bounds of performance enhancement in PDH PBMRs. Finally, we also make an illustrative comparison of our convenient isothermal model with a more detailed nonisothermal 2-D model to confirm the validity of our main assumptions.

Modeling of PDH Membrane Reactors

Governing equations for isothermal operation

The present PBMR model features the addition of membrane flux to a conventional PBR model (Figure 1). The governing equations for any component on each side of the PBMR are

$$\frac{dF_t}{dz} = r g'_{cat} - Q \cdot (P_t - P_s) 2\pi R_1 \quad \text{(Tube)} \tag{1}$$

$$\frac{dF_s}{dz} = Q \cdot (P_t - P_s) 2\pi R_1 \quad \text{(Shell)} \tag{2}$$

Here, F, Q, P, and R_1 represent molar flow rate (mol s^{-1}), membrane permeance (mol s^{-1} m^{-2} Pa^{-1}), pressure (Pa), and tube radius (m), respectively. The subscripts t and s denote the tube and the shell sides. The r term denotes the reaction kinetics and g'_{cat} refers to mass of catalyst per unit reactor length (g/m). The above governing equations are derived from material balance equations for each component (propane, propylene, and hydrogen). For most of the following discussion, we assume isothermal operation, plug flow inside the tube, no axial dispersion, and no radial diffusion. A discussion confirming the general validity of these assumptions in PDH PBMRs is presented toward the end of this article. The mass-transfer resistance of the membrane support and the pressure drop in the packed bed are neglected. To solve the governing equations, we use the explicit Euler method for the cocurrent mode and the implicit one-step modified Rosenbrock method[26] for the countercurrent mode. The total pressure on the tube and the shell side is kept constant, typically at 1 atm. At each step position along the reactor length, the partial pressures of the components on the tube and the shell are calculated (from the molar flow rates of each component), and the membrane flux is updated by multiplying these partial pressure differences with the component permeance Q. The membrane thickness is much smaller than the reactor radius, and hence for simplicity we use the same R_1 in the governing equations for both the tube and shell sides.

There are several papers describing the mechanisms for PDH reaction on chromium oxide-based and platinum-based catalysts.[2,27,28] In this study, we used the known Langmuir–Hinshelwood kinetics model for PDH on a Pt-Sn/Al_2O_3 catalyst. In this model, propane is physisorbed on Pt-Sn, followed by step-by-step dehydrogenation reactions on the

surface, and finally, the desorption of chemisorbed propylene and hydrogen.[27] This mechanism is described by the following overall rate equation

$$r = \frac{k_1\left(P_{C_3H_8} - 1/K_{eq}(P_{C_3H_6}P_{H_2})\right)}{\left(1+K_{C_3H_6}P_{C_3H_6}+(K_{H_2}P_{H_2})^{0.5}\right)^2} \quad (3)$$

Here, k_1 is the forward reaction rate (mol s^{-1} $g_{cat}{}^{-1}$ kPa^{-1}), K_{eq} is the temperature-dependent kinetic equilibrium constant, and K_i are the adsorption constants on the Pt-Sn surface. The temperature-dependent kinetic parameters are obtained from the rate constants and activation energy parameters given by Li et al.,[27] and our assumed reaction temperature is 600°C. We define propane conversion as

$$\text{Conversion} \equiv \frac{\text{Feed}_{C_3H_8} - \text{Total outlet}_{C_3H_8}}{\text{Feed}_{C_3H_8}} \quad (4)$$

The conversion is calculated accounting for the total outlet mole flow rate of propane including both the tube and shell (due to membrane permeation) side.

Dimensional analysis

To gain insight into the PBMR performance in a wide range of operating conditions, we nondimensionalize the governing equations using a characteristic flow rate and length, which are the feed flow rate (F) and reactor length (L), respectively

$$\frac{d(\tilde{v}_t y_t)}{d\tilde{z}} = Da\left(\frac{\left(y_{C_3H_8} - P_{total}/K_{eq}(y_{C_3H_6}y_{H_2})\right)}{\left(1+K_{C_3H_6}P_{C_3H_6}+(K_{H_2}P_{H_2})^{0.5}\right)^2}\right) - \frac{1}{Pe}\alpha\left(y_t - R_p y_s\right) \quad \text{(Tube)} \quad (5)$$

$$\frac{d(\tilde{v}_s y_s)}{d\tilde{z}} = \frac{1}{Pe}\frac{\alpha}{R_s}\left(y_t - R_p y_s\right) \quad \text{(Shell)} \quad (6)$$

$$\sum y_t = 1, \ \sum y_s = 1 \quad (7)$$

$$\left(\begin{array}{l} Da = \dfrac{k_1 R_g T(1-\varepsilon)L\rho_{cat}}{v_{t0}}, Pe = \dfrac{v_0}{Q_{H_2}\cdot R_g T}\dfrac{R_1}{2L} \text{ or } \dfrac{v_0\delta_{mem}}{D_{H_2}}\dfrac{R_1}{2L}, \\ \alpha_i = \text{membrane selectivity } (Q_i/Q_{H_2}), \\ R_s = \dfrac{\text{sweep flow rate}}{\text{feed flow rate}}, R_p = \dfrac{\text{Permeate pressure}}{\text{Retentate pressure}} \end{array}\right) \quad (8)$$

The mole fractions of each component are represented by y on the tube and shell sides. Da (the Damköhler number) represents the ratio of reaction rate and convective flow rate, and Pe (the Péclet number) describes the ratio of membrane flux and convective flux. It should be noted that the diffusivity used in Pe refers to diffusion of H_2 in the membrane, and hence this Pe is different from a gas-phase mass-transfer Pe inside the tube (which does not appear in the governing equations). The Pe defined here is the ratio of membrane permeance and weight hourly space velocity (WHSV, h^{-1}), or alternatively the ratio of g_{cat} and membrane surface area. The permeance used in Pe is that of hydrogen, and the membrane selectivity α_i is the permeance of component i divided by the hydrogen permeance. For example, α_i is zero if the membrane does not allow propane and propylene permeation, thus corresponding to perfect H_2 selectivity. The parameter R_s represents the ratio of sweep and feed volumetric flow rates. The parameter R_p is the ratio of permeate and retentate total pressure. The above methods of nondimensionalization are broadly consistent with those carried out in the previous PBMR modeling literature.[18,19,25]

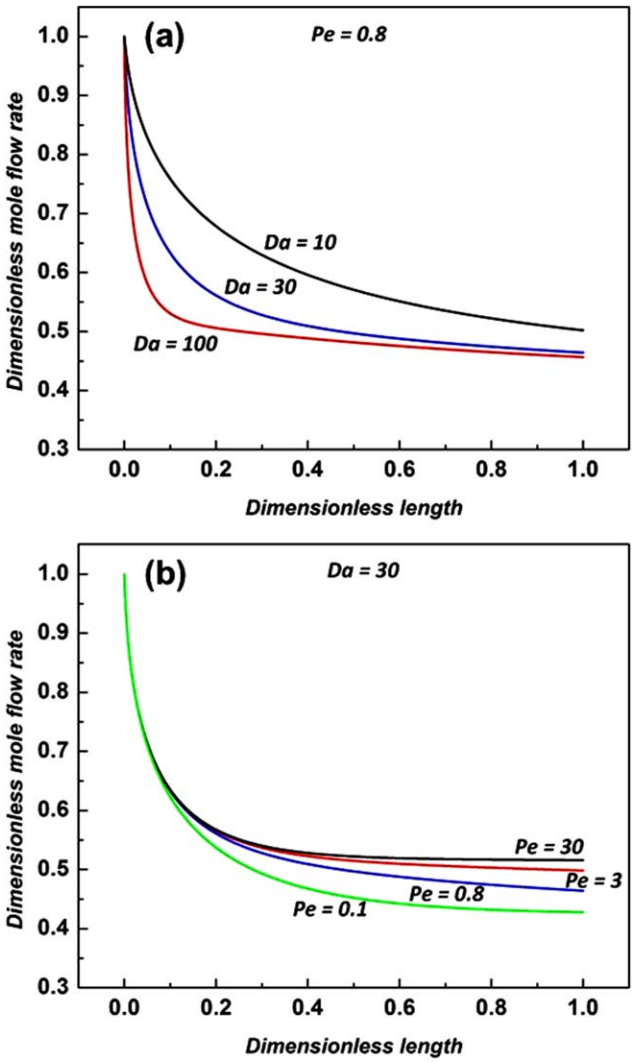

Figure 2. Dimensionless propane flow rate along the reactor at fixed (a) *Pe* and (b) *Da* ($\alpha = 0$, $R_s = 1$, $R_p = 1$).

[Color figure can be viewed in the online issue, which is available at wileyonlinelibrary.com.]

Results and Discussion

As shown in Eqs. 5–8, the governing relations become functions of Pe, Da, α (membrane selectivity), R_s (ratio of volumetric sweep and feed flow rates), and R_p (ratio of pressures at the tube and shell side). For fixed α, R_s, and R_p, the results can be represented by Pe and Da regardless of reactor size, thus allowing 2-D "operating window" plots for the PBMR performance. Before showing these plots, we briefly discuss a few typical results of the simulation at given Pe and Da values. Figure 2 shows the dimensionless mole flow rate of propane along the reactor with different Da and Pe. As Da relates reaction kinetics to space velocity, it determines the initial slope of the dimensionless flow rate as shown in Figure 2a. The larger the Da, the faster the decrease of flow rate observed near the reactor entrance; whereas smaller Pe values further decrease the flow rate of propane due to membrane permeation after the initial decrease. At

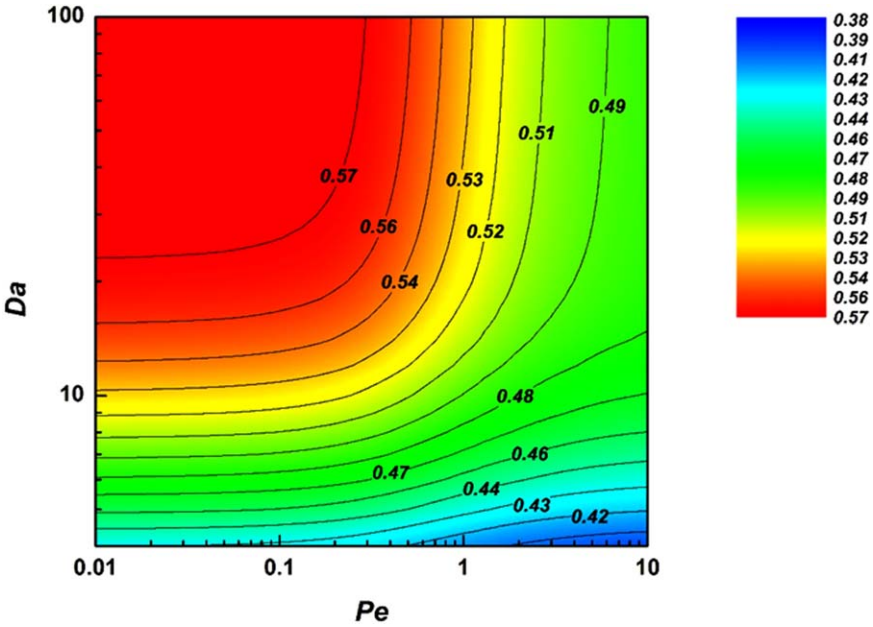

Figure 3. Operating window for PDH PBMRs using hydrogen-selective membranes ($\alpha = 0$, $R_s = 1$, $R_p = 1$). The color scale depicts the PBMR conversion.

[Color figure can be viewed in the online issue, which is available at wileyonlinelibrary.com.]

infinite *Pe* (i.e., no membrane permeation), the equilibrium PDH conversion is reached. As seen in Figure 2b, enhancement of conversion using the PBMR is achieved by decreasing *Pe* (i.e., increasing the membrane permeation rate).

Effect of membrane properties

The membrane material for conversion enhancement in the PBMR ideally would have high PDH product permeability, high PDH product selectivity, and high temperature stability. Conventional polymeric membranes[29–31] are not viable at high temperatures, and inorganic membranes are essential. Various types of ceramic or metallic membranes for propylene-selective or hydrogen-selective separation have been reported.[32–35] One of the promising candidates are zeolite membranes, which have well-defined crystalline pore structures and for which membrane fabrication processes have been developed over two decades. Detailed studies of hydrogen-selective[36,37] and propylene-selective[38–41] zeolite membranes have been published. We compare three different types of membranes, namely small-pore zeolite membranes, medium-pore zeolite membranes, and large-pore Knudsen permeation membranes. In this section, we fix the volumetric sweep flow rate to be the same as the feed flow rate ($R_s = 1$) and consider the effect of the membrane properties. The small-pore zeolite membranes are assumed to have negligible permeances of the olefin and paraffin. The silicoaluminophosphate zeolite SAPO-34 (~0.38-nm pore size) is one example of a material with these properties.[9] The medium-pore zeolite membranes also allow propane and propylene to permeate, and are exemplified by MFI (~0.55-nm pore size) membranes.[9] The mesoporous membranes have larger pores (>2 nm) with Knudsen selectivity. They allow transport of all the three components with large permeances.

Figure 3 shows the operating window wherein the calculated conversions are displayed as a color-coded contour plot with respect to a wide range of *Da* and *Pe*. These results are for small-pore hydrogen-selective zeolite membranes wherein α is zero for propane and propylene. One can easily conclude that higher conversion can be achieved by increasing *Da* and lowering *Pe*. In the low-*Da* region, the system becomes kinetic-controlled while in the high-*Da* region the conversion is strongly affected by the *Pe* value in the range of 0.1–10. In this region, membrane permeation becomes effective in breaking the equilibrium limitation. There exists a plateau region at $Da > 20$ and $Pe < 0.1$ in which there is no further conversion enhancement. This behavior is due to the decreasing membrane permeation along the reactor length. Although enhanced membrane permeation lowers *Pe*, it also increases the shell-side hydrogen concentration and thus decreases the

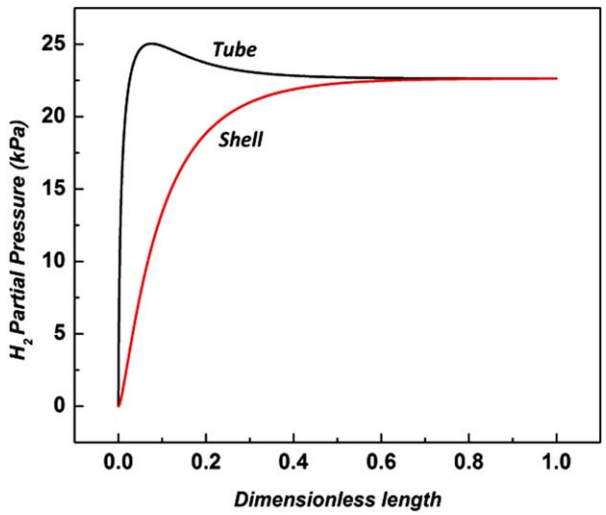

Figure 4. Partial pressure profiles of hydrogen along the PBMR length at the tube and the shell sides, with $Pe = 0.1$ and $Da = 80$ ($\alpha = 0$, $R_s = 1$, $R_p = 1$).

[Color figure can be viewed in the online issue, which is available at wileyonlinelibrary.com.]

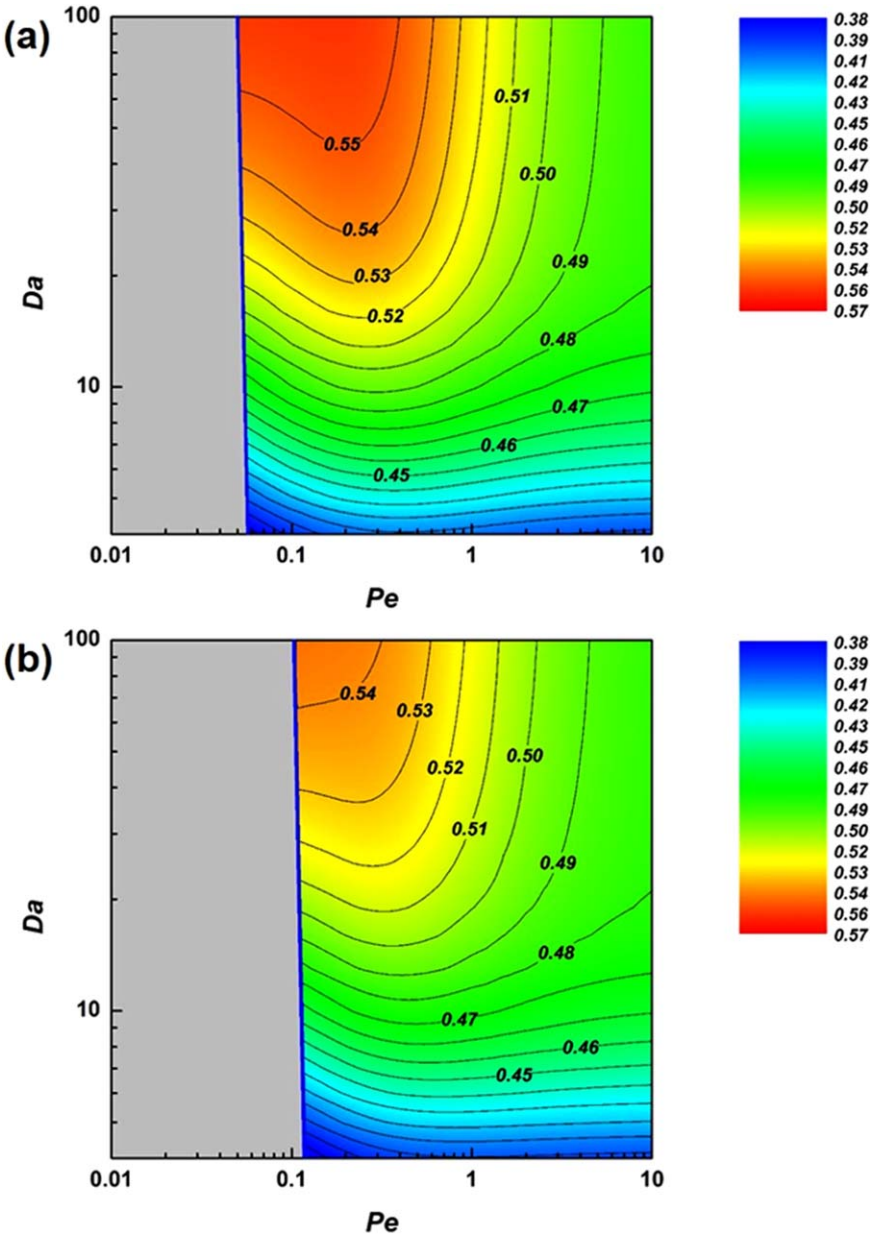

Figure 5. Operating windows for PDH PBMRs using (a) medium-pore ($\alpha = 0.1$) and (b) large-pore (Knudsen, $\alpha = 0.2$) membranes. The "nonoperating" regions are shaded in gray. The color scale depicts the PBMR conversion.

[Color figure can be viewed in the online issue, which is available at wileyonlinelibrary.com.]

permeation driving force (the partial pressure difference of H_2 between the tube and shell sides) as the feed flow proceeds down the reactor length. Increasing the membrane permeation assists enhancement near the reactor inlet, but eventually the differences in mole fraction between the tube and the shell side become small, and there is little membrane permeation downstream as shown in Figure 4. This highlights an important fact that the degree of enhancement in the PBMR will be limited unless other factors such as feed composition, sweep flow rate (R_s), or operating configuration itself, are changed. We discuss this further in the next section.

We also consider other types of membranes, as mentioned earlier. The most commonly used large-pore ceramic membranes follow Knudsen diffusion due to their relatively large pore size (2–200 nm). The Knudsen selectivity is determined by the square root of the ratio of the component molecular weights. The H_2/C_3H_8 and H_2/C_3H_6 selectivities are about 4.7 and hence α is about 0.2 for both the olefin and paraffin. For medium-pore zeolite membranes such as MFI, α is about 0.1 for both the olefin and paraffin.[42–44] Figure 5 shows the operating windows for these two values of α. Both windows are calculated with the same assumptions as for the hydrogen-selective membranes. We find that there exist "nonoperating regions," which are shown in gray color. The boundary lines between the operating and nonoperating regions represent the "depletion line" of propane, which is zero flow rate of propane on the retentate (tube) side. This condition occurs when all the propane feed gas is consumed by membrane permeation and catalytic reaction. Hence, the calculated conversions in the nonoperating region are not physically meaningful.

Figure 5 also indicates narrower operating regions for medium-pore and larger-pore membranes. It should be noted

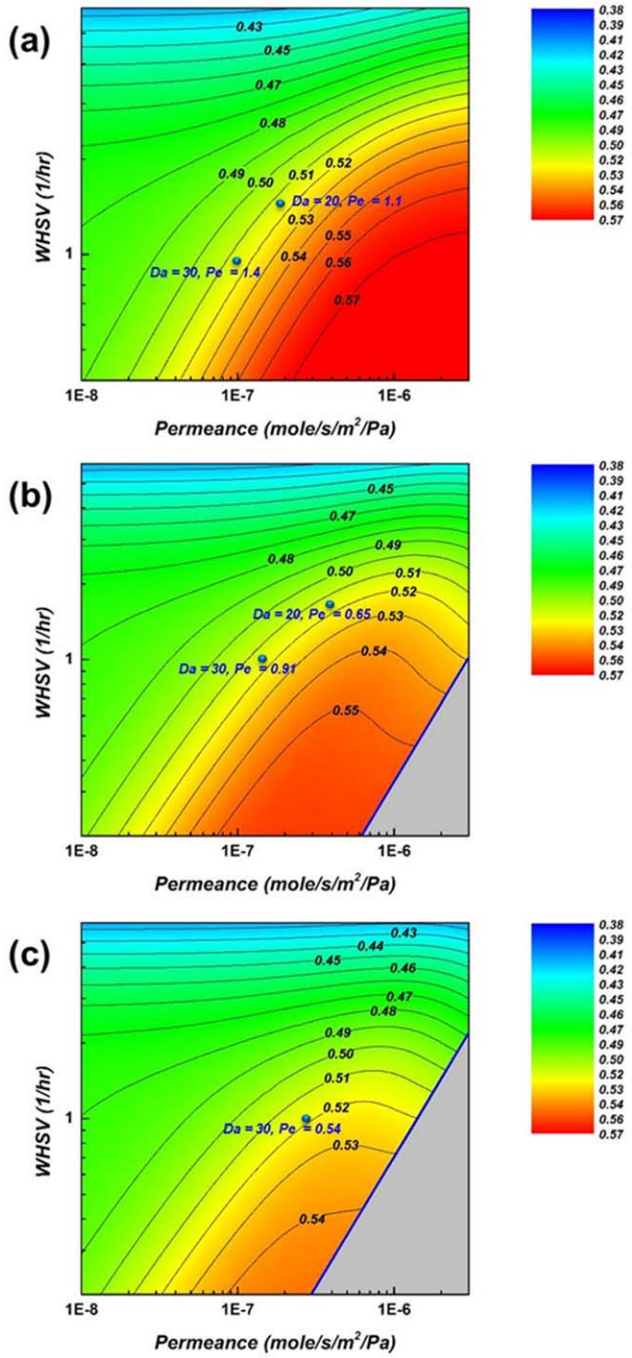

Figure 6. Operating windows for PDH PBMRs using membrane permeance and WHSV for (a) small-pore ($\alpha = 0$), (b) medium-pore ($\alpha = 0.1$), and (c) Knudsen ($\alpha = 0.2$) membranes ($R_1 = 0.0035$ m, $L = 0.1$ m). The color scale depicts the PBMR conversion.

[Color figure can be viewed in the online issue, which is available at wileyonlinelibrary.com.]

that if the propane is completely consumed in a certain length of the reactor, the propane on the shell side can back-permeate to the tube side in the remaining downstream length. However, this is not considered here as such a reactor operation condition is not practical. Compared to the case of hydrogen-selective membranes, the operating windows in Figure 5 do not show a plateau region. Instead, there exist maximum values of the conversion at each *Da*. Although low values of *Pe* generally enhance conversion, the propane reactant also permeates through the membrane thus forcing the equilibrium backward. Hence, there is a trade-off between reactant and product permeation. The trends seen in Figures 3 and 5 for PDH are consistent with those seen in Harold et al. for cyclohexane dehydrogenation.[18] In that work, it was shown that there exist optimum ratios of permeation and reaction rates for certain values of membrane selectivities. Furthermore, for an infinitely hydrogen-selective membrane, the cyclohexane conversion reached a plateau with increasing permeation rate. Here, we have examined this trend in the context of PDH for a much wider range of *Da* (ratio of reaction rate and convective transport rate), so that we can clearly identify the optimum value of *Pe* at each *Da* of practical interest. Among the different types of membranes, hydrogen-selective membranes show the best performance as they allow negligible permeation of the propane reactant, even though they also retain the propylene product on the tube side. Hence, membranes made of small-pore zeolites such as DDR or SAPO-34 are likely the best candidates for PDH PBMR applications, but medium-pore zeolite or larger-pore Knudsen-selective membranes also show some level of enhancement. In the case of Knudsen-selective membranes one should consider the reactant/product permeation trade-off and the narrower operating region allowed.

Using the definitions of *Pe* and *Da* and assigning reactor dimensions (e.g., $R_1 = 0.35$ cm and $L = 10$ cm, which are typical dimensions of ceramic tubes used for PDH PBMRs), we can extract dimensional process variables such as the WHSV (h^{-1}) and the membrane permeance (mol s^{-1} m^{-2} Pa^{-1}), which are two important parameters for PBMR application. Using Figure 6, we can deduce the range of WHSV and membrane permeance required for a target conversion. For example, we can obtain 55% PDH conversion using small-pore zeolite membranes with a required permeance range of 2–6 $\times$ 10^{-7} mol s^{-1} m^{-2} Pa^{-1} if the PBMR is operated at WHSV 1–1.5 h^{-1}. This H_2 permeance can be achieved by fabricating membranes about 1 μm thin, considering that the previously reported H_2 permeance of SAPO-34 and DDR membranes is about 5 $\times$ 10^{-8} mol s^{-1} m^{-2} Pa^{-1} with 5–10 μm thickness.[45,46] This type of information is important for PBMR evaluation, and for appropriate material selection or design.

Effects of sweep flow rate

As discussed in the previous section, the PBMR shows a plateau region in which there is no further conversion enhancement. This is because of the increase in hydrogen concentration at the shell side due to membrane permeation, thereby decreasing the driving force for further permeation. A simple way of overcoming this limitation is to increase the sweep flow rate in order to decrease the mole fraction of hydrogen in the permeate and hence allow more membrane permeation for the same *Pe*. This is represented in Figure 7 using a sweep flow rate of $R_s = 3$, three times larger than the calculations shown earlier. The other parameters are the same as in the previous case of hydrogen-selective membranes. In Figure 7, conversion increases significantly to a plateau of 66% as compared to 57% in the case of $R_s = 1$. However, the conversion enhancement by increasing the

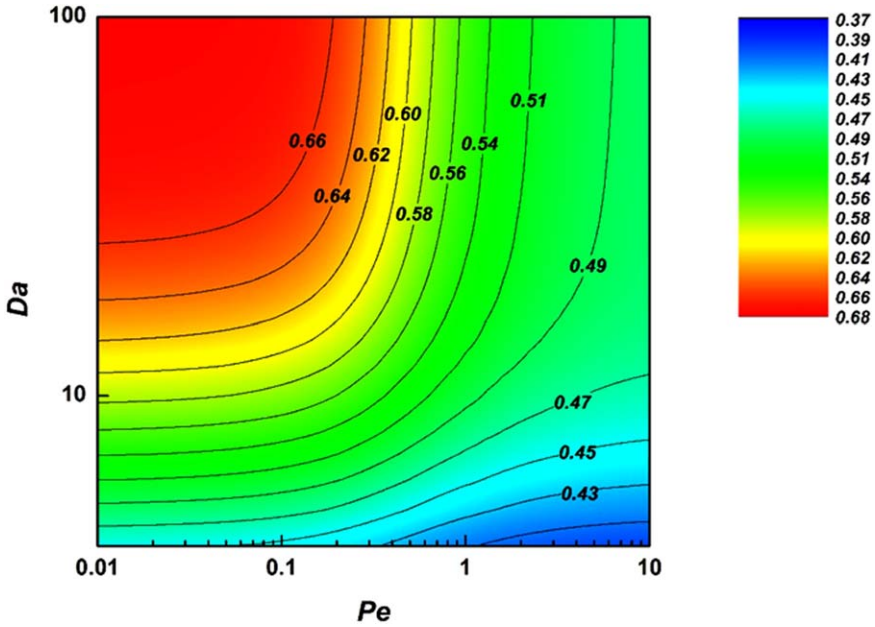

Figure 7. Operating window for PDH PBMRs using hydrogen-selective membranes with a large sweep flow rate, corresponding to parameters $\alpha = 0$, $R_s = 3$, and $R_p = 1$. The color scale depicts the PBMR conversion.

[Color figure can be viewed in the online issue, which is available at wileyonlinelibrary.com.]

sweep flow rate should be weighed appropriately against the increase in the operating cost of the PBMR.

Effects of pressure ratio

The total pressures of both the tube and shell side are maintained at 1 atm ($R_p = 1$), primarily because the equilibrium conversion of the dehydrogenation reaction decreases with increasing pressure. The driving forces for membrane permeation are the partial pressure differentials of each component between the tube and shell side, rather than the total pressure differential across the membrane. However, the membrane fluxes would be increased using a higher total pressure at the tube side or lowering the pressure at the shell side. Gokhale et al. have discussed the effect of pressure ratio on isobutane dehydrogenation in a PBMR, and showed a conversion increase with decreasing pressure ratio.[19] However, this trend is only valid if the total pressure at the shell side is decreased while the tube pressure is maintained at 1 atm. Pressurizing the feed (tube) side will lead to decrease conversion with decreasing pressure ratio, which is opposite to Gokhale et al. even with the same pressure ratio. There will be more increase in product concentrations than that of

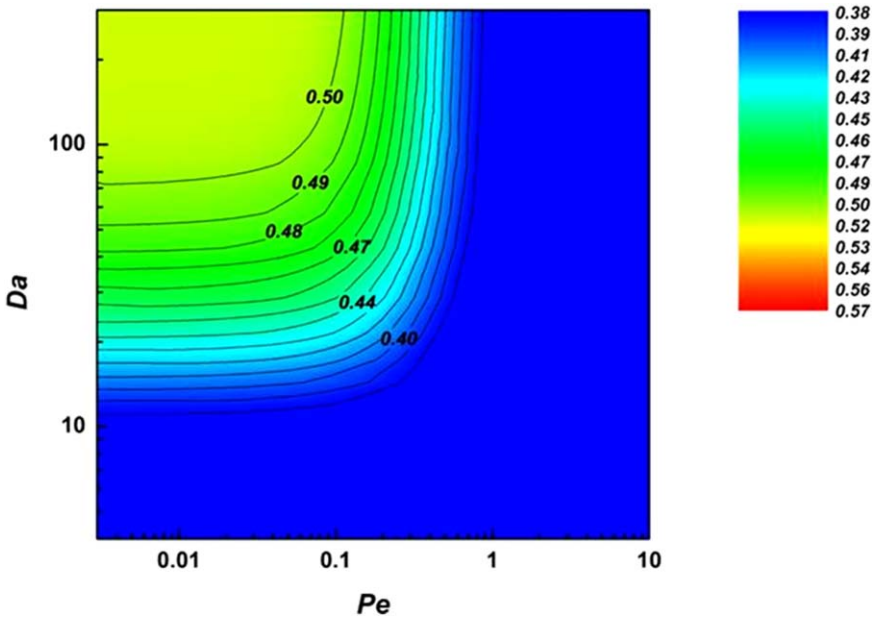

Figure 8. Operating window for PDH PBMRs using hydrogen-selective membranes with a large pressure at tube (3 atm, $R_p = 0.33$), corresponding to parameters $\alpha = 0$ and $R_s = 1$. The color scale depicts the PBMR conversion.

[Color figure can be viewed in the online issue, which is available at wileyonlinelibrary.com.]

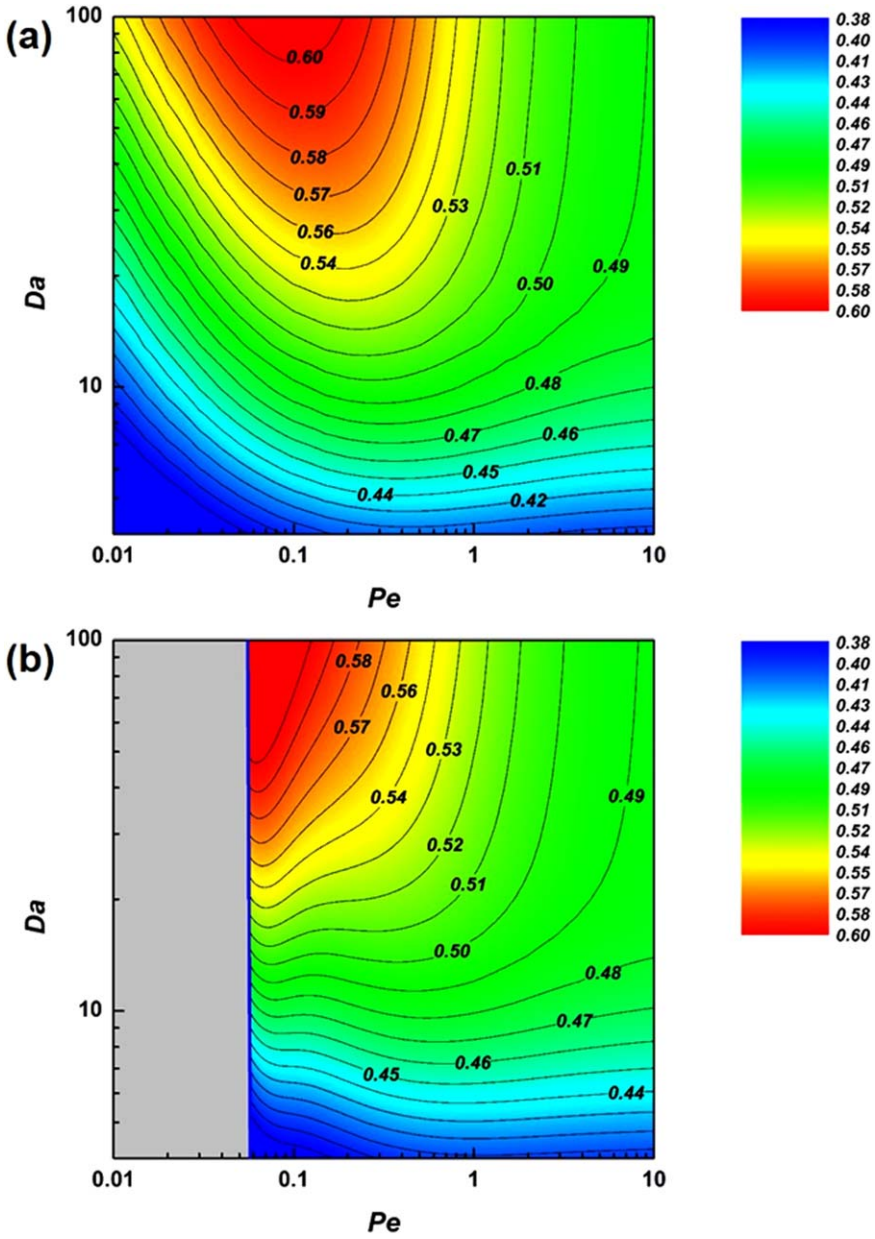

Figure 9. Operating windows for PDH PBMRs using (a) hydrogen-selective ($\alpha = 0$) and (b) medium-pore ($\alpha = 0.1$) membranes in countercurrent sweep gas mode. The color scale depicts the PBMR conversion.

[Color figure can be viewed in the online issue, which is available at wileyonlinelibrary.com.]

the reactant, leading to an equilibrium shift to the reactant side. In large-scale PDH processes, applying a vacuum on the permeate side is not considered cost-effective. *Pe* decreases and *Da* increases with increasing total pressure at the tube side, but the reverse reaction in the dimensionless reaction term will be increased as well, which is not favorable for conversion. Figure 8 shows the operating window at a larger tube pressure (3 atm, $R_p = 0.33$) with the shell side at 1 atm, and it clearly indicates that the equilibrium shift away from the products is more significant than increased membrane permeation. Therefore, we consider atmospheric-pressure operation as the most practical case in this paper.

Effect of sweep gas modes

The results presented in the foregoing sections all assumed a cocurrent sweep gas mode. Another potential way of enhancing PBMR performance is the use of a countercurrent sweep gas mode. In the countercurrent case, the governing equation remains the same for the tube side. For the shell side, the flow direction is reversed and the governing equation is slightly modified

$$-\frac{d(\tilde{v}_s y_s)}{d\tilde{z}} = \frac{1}{Pe}\cdot\frac{\alpha}{R_s}\,(y_t - y_s) \qquad \text{(Shell)} \tag{9}$$

The variables on the shell side are unknown at the reactor entrance ($z = 0$), so the simulations are repeated with different assumed values at the entrance, and iterated until the known sweep gas conditions at the exit ($z = 1$) are achieved. Then, the operating window for countercurrent mode can be drawn as shown in Figure 9 for both medium-pore ($\alpha = 0.1$) and hydrogen-selective ($\alpha = 0$) membranes, and can be compared to the cocurrent mode (Figures 3 and 5). It is seen that

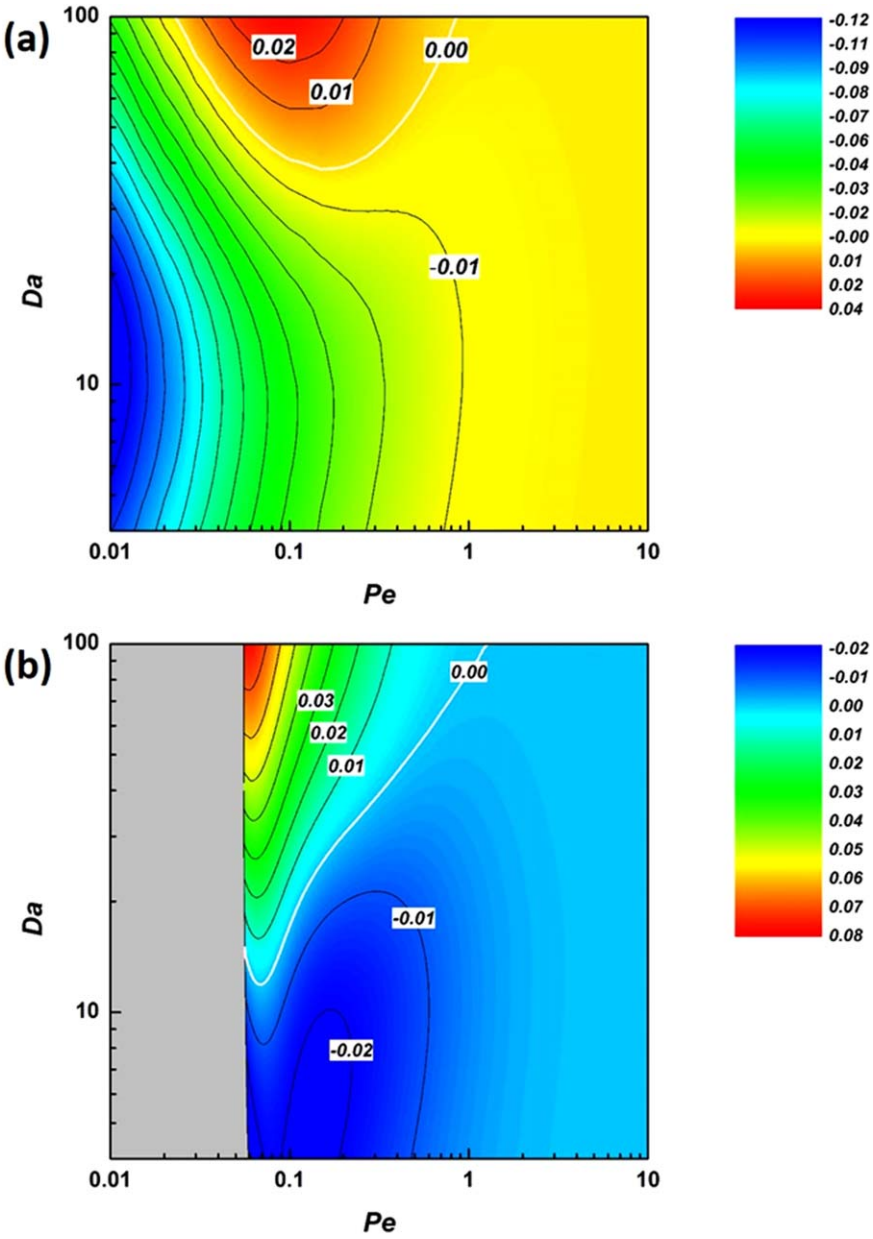

Figure 10. Difference in PBMR conversion between countercurrent and cocurrent sweep gas modes for (a) hydrogen-selective ($\alpha = 0$) and (b) medium-pore ($\alpha = 0.1$) membranes. The color scale depicts the PBMR conversion.

[Color figure can be viewed in the online issue, which is available at wileyonlinelibrary.com.]

the depletion line of propane for medium-pore membranes still remains in the case of countercurrent operation. There is a very strong dependence of conversion on *Da* near the depletion line as the depletion of propane due to membrane permeation is also strongly affected by the feed flow rate. The difference in conversion between countercurrent and cocurrent modes is shown in Figure 10. The cocurrent mode shows better performance for most of the range of operating conditions, as can be seen in Figure 10. Only at high *Da* and low *Pe* does the countercurrent mode overcome the plateau region seen in the cocurrent mode. Unlike the cocurrent mode, continuous membrane permeation along the reactor length can be achieved using countercurrent mode as shown in Figure 11. However, although the countercurrent sweep gas decreases the hydrogen concentration more effectively near the sweep gas entrance ($z = 1$), there is also a back-permeation of hydrogen from the shell to the tube side near the feed gas entrance due to higher partial pressure in the shell side (Figure 11), thereby decreasing the MR conversion. It was believed that the countercurrent sweep mode better eliminates gas concentrations in the shell side, similar to the countercurrent heat exchanger concept. Gallucci et al. showed modeling results at a particular operating condition, wherein continuous hydrogen permeation along the reactor is observed.[24] This is consistent with Figure 11, but in terms of the PBMR performance a significantly higher conversion with countercurrent sweep can be only achieved in a limited operating range of high *Da* ($\sim$100) and low *Pe* ($\sim$0.1).

Figure 12 shows the difference of dimensionless propane flow rate between cocurrent and countercurrent sweep gas modes, with *Pe* and *Da* indicated. In Figure 12a, a smaller decrease in flow rate is observed at $Pe = 0.1$ and $Da = 20$

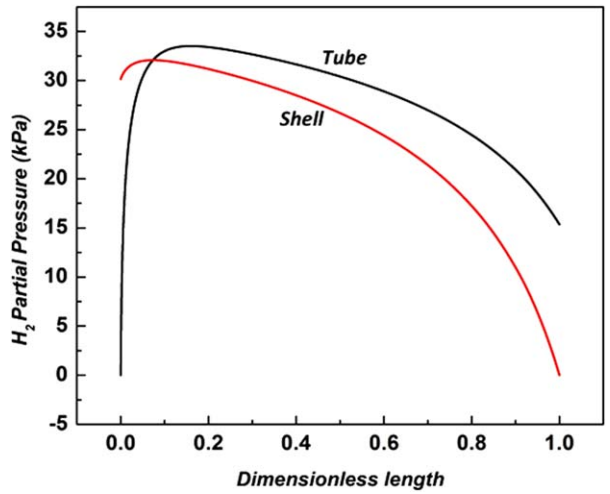

Figure 11. Partial pressure profiles of hydrogen along the reactor length at the tube and the shell side in countercurrent sweep gas mode using hydrogen-selective ($\alpha = 0$) membranes ($Pe = 0.1$ and $Da = 80$).

[Color figure can be viewed in the online issue, which is available at wileyonlinelibrary.com.]

for the countercurrent mode near the feed gas entrance, due to hydrogen back-permeation in that region. However, there is a greater propane flow decrease in countercurrent mode near the reactor exit, which is because of the effective removal of hydrogen. When Pe drops to 0.01, we observe more decrease in propane flow rate in countercurrent than the concurrent mode. However, at $Da = 20$, the more effective hydrogen removal still cannot overcome the effect of hydrogen back-permeation and shows a smaller decrease of propane feed flow rate overall, thus ending up with a lower conversion. Conversely, Figure 12b shows that for $Pe = 0.1$ and $Da = 80$, the hydrogen back-permeation still exists but the countercurrent hydrogen removal overcomes this negative effect and attains a higher conversion. It should be mentioned that further decreasing Pe, for example, to 0.02 as shown in Figure 12b, leads to lower conversion as it further increases the hydrogen back-permeation. In summary, a high Da is always necessary for the countercurrent mode as the reaction kinetics should be fast enough to compensate for the negative effect of hydrogen back-permeation. A low Pe is also required for effective hydrogen removal, but a Pe that is too low will cause undesired hydrogen back-permeation. Therefore, a trade-off relation exists between effective hydrogen removal and its own back permeation. Compared to the cocurrent mode, the operating window for the countercurrent mode shows considerable sensitivity to process conditions for $Pe < 0.1$, which implies there could be difficulties in process control of the countercurrent PBMR. However, it still suggests a possibility of enhancing PBMR performance by simply changing the direction of sweep flow, which does not increase the operating cost significantly.

Shell-side catalyst

In this section, we consider another PBMR configuration, in which the packed catalyst bed is placed on the shell side and permeate gases are collected in the membrane tubes. The governing equations are slightly modified, and we use

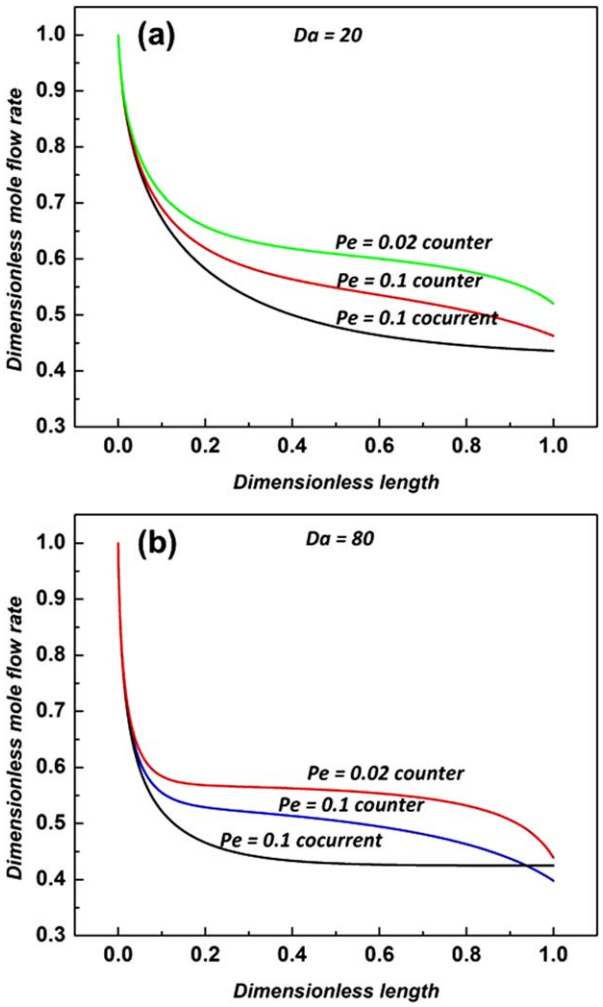

Figure 12. Dimensionless propane flow rates for cocurrent and countercurrent sweep modes using hydrogen-selective ($\alpha = 0$) membranes, with (a) $Da = 20$ and (b) $Da = 80$.

[Color figure can be viewed in the online issue, which is available at wileyonlinelibrary.com.]

one more parameter, which is the number of membrane tubes (n) for a given amount of shell-side catalyst. The dimensionless governing equations remain the same, but the definition of Pe changes when considering permeation through n tubes. Assuming the same total volumetric flow rate and g_{cat}, and the same radius of membrane tubes (R_1), the Pe for a PBMR using n tubes can be defined as

$$Pe = \frac{v_{t0}}{Q_{H_2} R_g T} \frac{R_1}{2L} \frac{1}{n} \tag{10}$$

The definition of Da remains unchanged. The operating windows shown in previous figures do not change, as the same governing equations still apply. However, we can now alter the value of Pe by changing the value of n. As we increase n, the resulting lower Pe allows an increased conversion over the case of tube-side catalyst, for the same operating conditions and membrane properties. For example, if $Da = 20$ and $Pe = 4$, we expect to obtain about 49% conversion with a tube-side catalyst (Figure 3). For given reactor dimensions ($R_1 = 0.0035$ m, $L = 0.1$ m), the required WHSV is 1.5 h^{-1} and the membrane permeance is 8×10^{-8} mol s^{-1} m^{-2} Pa^{-1}. However, if five tubes are used

Table 1. Required *Pe* and Membrane Permeances (in mol s^{-1} m^{-2} Pa^{-1}) at Different Fixed *Da* (and Hence WHSV) Values, for a Target 52% PBMR Conversion ($R_1 = 0.0035$ m, $L = 0.1$ m)

	Da = 30 (WHSV = 0.95)			*Da* = 20 (WHSV = 1.43)			*Da* = 10 (WHSV = 2.87)		
	$\alpha = 0$	$\alpha = 0.1$	$\alpha = 0.2$	$\alpha = 0$	$\alpha = 0.1$	$\alpha = 0.2$	$\alpha = 0$	$\alpha = 0.1$	$\alpha = 0.2$
Pe	1.38	0.91	0.54	1.12	0.65	n.a.	0.24	n.a.	n.a.
Q ($\times 10^{-7}$)	0.96	1.6	2.8	1.8	3.7	n.a.	16	n.a.	n.a.

n.a.: Not Achievable.

with a shell-side catalyst, *Pe* becomes 0.8 and the conversion increases to 53% with the same membrane properties. This implies the potential of using multiple tubes in one unit if a membrane with a large permeance is not available. The *Pe* and *Da* can be defined using more familiar operating and material parameters such as WHSV and permeance

$$Pe = \frac{1}{P_{\text{total}}(mw_{\text{feed}})3600}\frac{\text{WHSV}}{Q_{H_2}}\frac{g_{\text{cat}}}{n2\pi R_1 L} \tag{11}$$

$$Da = P_{\text{total}}(mw_{\text{feed}})3600\frac{k_1}{\text{WHSV}} \tag{12}$$

Here, P_{total} is the tube-side total pressure, mw_{feed} (g mol^{-1}) is the molecular weight of the feed flow, and 3600 (s) is used for conversion to hourly flow rate. Because *Pe* includes the ratio of g_{cat} and membrane surface area, adding more tubes will increase the total membrane surface area, which leads to a lower *Pe*. For a certain conversion, the required *Pe* is determined at each *Da*, and the required ratio of g_{cat} and membrane surface area can then be calculated for a specific catalyst, membrane, and desired WHSV. As g_{cat} is proportional to the shell side volume, we can derive a characteristic length scale (λ) for the PBMR with multiple tubes as follows

$$\lambda \propto \frac{R_2^2 - nR_1^2}{nR_1} \tag{13}$$

Here, R_1 and R_2 are the radii of the membrane tubes and whole reactor vessel surrounding the shell-side catalyst, respectively. With increasing n, λ decreases and leads to greater surface area relative to the total tube volume. As higher conversion corresponds to smaller *Pe*, a smaller characteristic length to enhance the performance. This suggests the use of closely packed multiple membrane tubes or ceramic hollow-fiber tubes (which are currently available) as options for scale-up of PDH PBMRs.

Required membrane properties for a target conversion

The operating windows can be used for specifying the required membrane properties, catalyst properties, or reactor conditions to obtain a target conversion. As conventional PDH PBRs in commercial use operate with well-optimized catalysts, we focus on membrane properties in this article. If the reactor dimensions and catalyst for PDH are already determined, we can design the required membrane properties based on the operating windows. For example, we assume a concurrent PBMR conversion of 52% at 600°C as a moderate but significant target (about 10% enhancement from the equilibrium conversion of 48% with a pure propane feed). Table 1 shows the maximum *Pe* at three different values of *Da* to obtain the target conversion. These specific *Pe* and *Da* values are also superimposed in Figure 6. It should be noted that the permeances on the *x* axis of Figure 6 are chosen to be in the range achievable with current membrane fabrication technology (also see discussion later). Thus, the *Pe*, *Da* combinations highlighted in Figure 6 represent technologically feasible conditions. If the same reactor conditions and kinetics for the Pt-Sn catalyst are applied, the minimum required permeances of different types of membranes are calculated at each WHSV. One finds that the medium-pore ($\alpha = 0.1$) or Knudsen ($\alpha = 0.2$) membranes require more permeance than hydrogen selective membranes ($\alpha = 0$) to obtain the target conversion. The membrane permeance already includes the effect of thickness, so the required permeance can be achieved both by appropriate material selection and by controlling the membrane thickness. Considering that the high-temperature H_2 permeance range of zeolite membranes

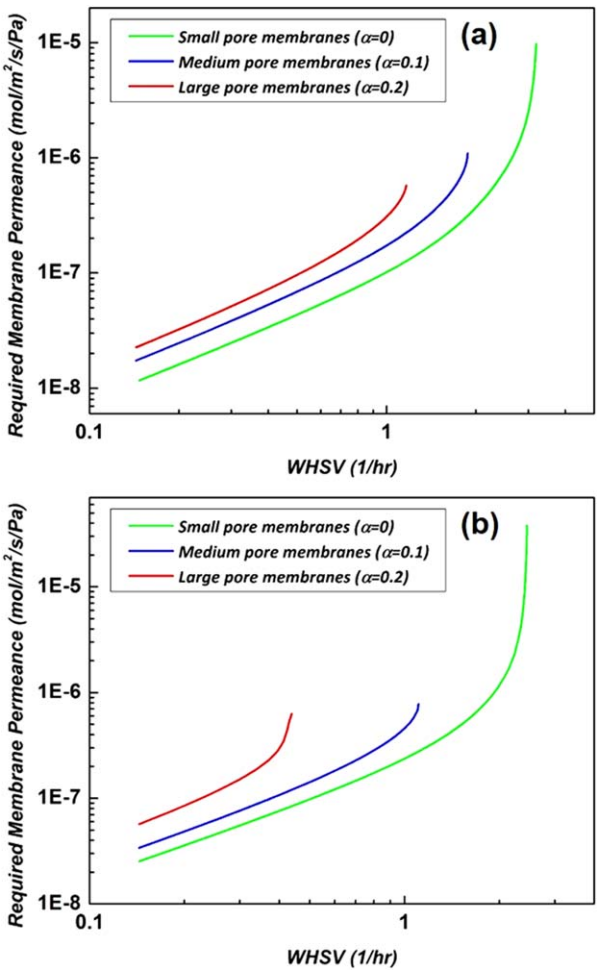

Figure 13. Required membrane permeances for targeted conversions of (a) 52% and (b) 54%, in PBMRs using all three types of membranes.

[Color figure can be viewed in the online issue, which is available at wileyonlinelibrary.com.]

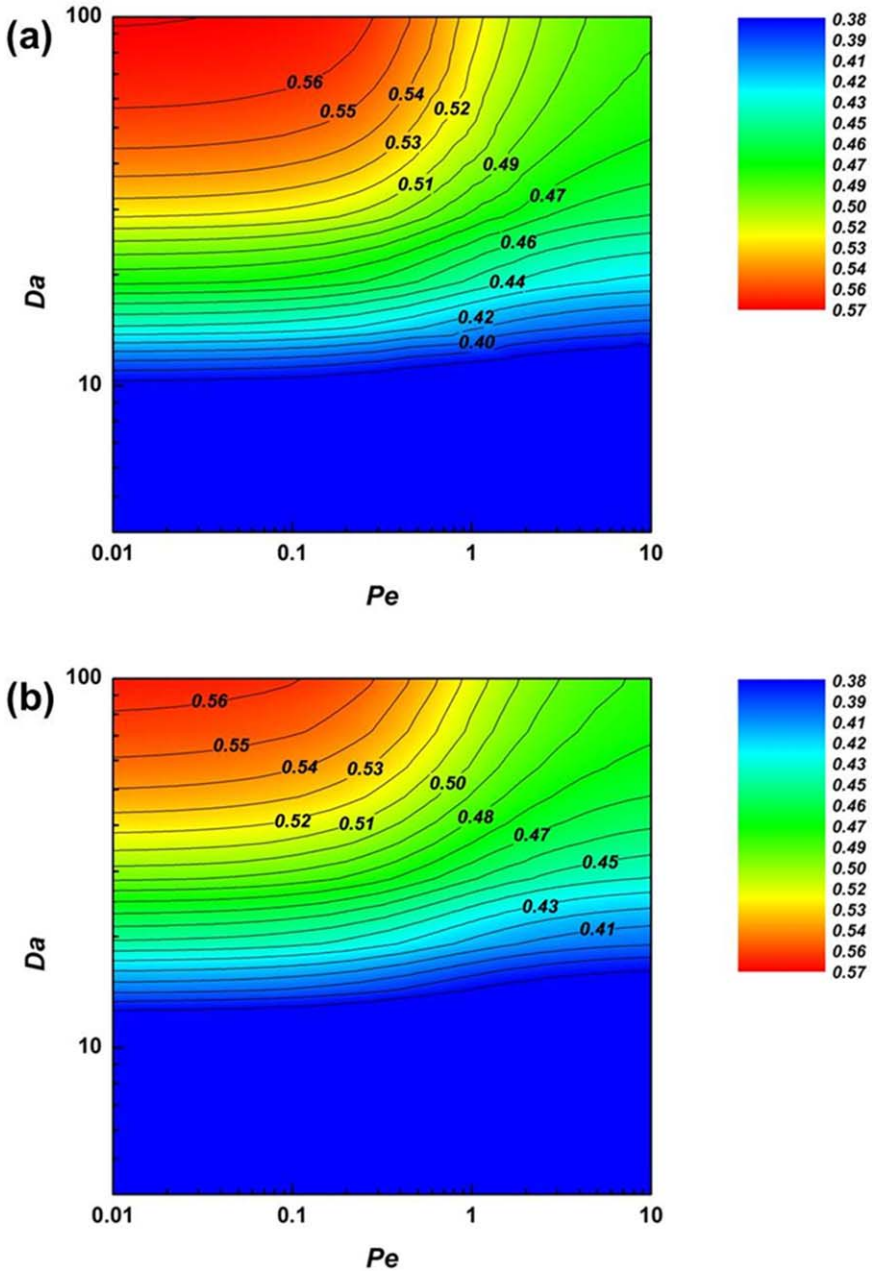

Figure 14. Operating window for PDH PBMRs using hydrogen-selective membranes with nonisothermal conditions of (a) nonadiabatic heat supply with fixed wall temperature ($T_w = 600^\circ$C) and (b) adiabatic operation, corresponding to parameters $\alpha = 0$, $R_s = 1$, and $R_p = 1$. The color scale depicts the PBMR conversion.

[Color figure can be viewed in the online issue, which is available at wileyonlinelibrary.com.]

is $10^{-8}-10^{-6}$ mol s^{-1} m^{-2} Pa^{-1} for an approximately 1–5 micron thickness range,[45–47] it appears that the required properties can be easily achieved for the target conversion at low WHSV <1 h^{-1}. However, if a larger WHSV (>2 h^{-1}) is used, medium-pore or Knudsen membranes will not be recommended as they cannot achieve the target conversion (Table 1).

Figure 13 shows the minimum permeances required for the three types of membranes in the WHSV range 0.1–5 h^{-1} for two different conversions. Medium-pore membranes such as MFI can be still used for WHSVs up to about 1.8 h^{-1} for a 52% conversion. However, if the target conversion is 54% the possible operating range of WHSV become significantly narrower especially for medium-pore and Knudsen membranes as described in Figure 13b. Small-pore membranes (e.g., SAPO-34), require relatively moderate membrane permeance for WHSV up to 2 h^{-1}, which can be achieved by fabrication of membranes of <2 micron thickness. At higher WHSVs, permeances higher than 10^{-6} mol s^{-1} m^{-2} Pa^{-1} are required. This result implies that reducing zeolite membrane thickness to the submicron regime while controlling membrane defects is an important opportunity and challenge for PBMR applications. Recent developments in hydrothermal zeolite membrane synthesis,[48] as well as fabrication of ultrathin membranes from 2-D zeolite materials,[49] offer useful directions for the pursuit of membrane thickness reduction.

Effects of simplifying assumptions

As stated in Introduction, we have assumed isothermal operation, no axial diffusion, and no radial dispersion. The isothermal assumption requires further analysis, as PDH is a highly endothermic reaction ($\Delta H = 125$ kJ mol^{-1}). To address this issue, we augment our model with a 2-D energy balance along with appropriate boundary conditions (Supporting Information). The mass- and heat-transfer equations are coupled and solved simultaneously, using realistic values for the heat-transfer parameters (Supporting Information) and the same PBMR dimensions as used in Table 1. The PBMR performance now cannot be understood solely as a function of *Pe* and *Da*, but is also a function of the heat-transfer parameters (whose numerical values are listed in Supporting Information). Moon and Park previously studied nonisothermal conditions for cyclohexane dehydrogenation.[25] However, parabolic temperature profiles were assumed along the reactor, with a maximum temperature of 493 K at the reactor axis. These assumptions clearly are not valid in PDH. Considering the fact that there are several different heat supply options, such as nonadiabatic heat supply from the outer wall or adiabatic operation with different preheating temperatures, there will be different types of operating windows.

Here, we illustrate the validity of our initial simplifying assumptions using the operating windows shown in Figure 14 for nonadiabatic and adiabatic operation. It is seen that nonisothermal operation (involving axial and radial temperature variations) shifts the conversion to lower values, but the qualitative trends remain the same over the range of practically useful *Da* and *Pe*. At small *Da*, the performance is mainly affected by *Da* as the system is kinetically controlled. However, *Pe* comes into effect after the system reaches equilibrium-limited conditions. It is worth mentioning that the region of $Da < 10$ (where large temperature drops are observed) shows almost no effect of *Pe*, and thus membrane permeation would not be useful. To avoid these conditions, a higher preheating temperature or higher wall temperature would typically be used.

Finally, the mass dispersion assumptions can be examined using the axial and radial mass-transfer Péclet numbers. Although the Péclet numbers depend on the mass dispersion coefficients which are not precisely known for the PDH PBMR, we can estimate that for a PDH PBMR tube of length $\sim$1 m operated at a typical WHSV of 1–10 h^{-1} at 600°C, the axial mass-transfer *Pe* would typically be $>>1$ and is not expected to have a significant effect. Conversely, the radial *Pe* should be much smaller than the axial *Pe* in order to avoid the deleterious effects of external mass-transfer resistance on the permeation rate. For PBMR tubes with $R_1/L \sim 10^{-2}$ as considered in this work, and for hollow-fiber PBMRs of even smaller radius, the effects of radial dispersion can be reasonably expected to be small. Overall, the simplified one-dimensional isothermal PDH PBMR model provides useful design guidelines for membrane material selection and operating conditions.

Conclusions

We have considered the "operating windows" of packed-bed membrane reactors (PBMRs) for PDH applications. Using a relatively simple isothermal model to set up dimensionless governing variables, we compared the operating ranges and reactor conversions for different types of membranes. Medium-pore zeolite and Knudsen-selective membranes show complex trends with *Pe*, whereas hydrogen-selective small-pore zeolite membranes show a plateau region of conversion at low *Pe*. This limitation can be overcome with different sweep gas operations, that is, larger sweep flow rate and countercurrent sweep gas mode. Obviously, a large sweep flow rate leads to more membrane permeation and thus increases conversion. However, use of the countercurrent sweep mode is more complicated as it has a trade-off relation between forward permeation and back-permeation of hydrogen, and it shows sensitivity to process conditions. We also consider another type of PBMR configuration, which is the use of shell-side catalyst. This is predicted to show better performance than a PBMR with a tube-side catalyst, as *Pe* can now be adjusted by altering the number of membrane tubes that collect the permeate.

As far as the membrane material selection is concerned, small-pore zeolite membranes would be preferred over medium-pore and Knudsen membranes, as they provide a wider range of WHSV for the PBMR operation to achieve a target conversion. However, they have a lower permeability due to their small (<0.4 nm) pores, and hence require reliable fabrication in the form of micron-thin or submicron membranes. Although hydrogen-selective small-pore membranes are preferred, the medium-pore and Knudsen membranes do provide moderate enhancement of PBMR performance at low WSHV < 1 h^{-1}. The nonisothermal operating windows show a shift of conversion to lower values especially at small *Da* where heat supply is poor; however, the general trends of PBMR performance remain the same. Our consideration of the PDH PBMR in terms of operating windows thus provides useful guidelines for overall design of the PBMR system as well as for selection and design of appropriate membrane materials and fabrication processes. This method should also be easily transferrable for other dehydrogenation reactions (e.g., ethane and *iso*-butane).

Notation

F_t = mole flow rate at the tube, mol s^{-1}
F_s = mole flow rate at the shell, mol s^{-1}
g'_{cat} = amount of catalyst in unit length, g m^{-1}
k_1 = forward reaction rate, mol s^{-1} g$_{cat}^{-1}$ kPa^{-1})
K_{eq} = equilibrium parameter, kPa^{-1}
K_i = isotherm parameter for species *i*, kPa^{-1}
P_t = pressures in the tube side for each component, kPa
P_s = pressures in the shell side for each component, kPa
y_t = mole fractions in the tube side for each component
y_s = mole fractions in the shell side for each component
Q_i = membrane permeance for species *i*, mol s^{-1} m^{-2} Pa^{-1}
R_1 = the radius of membrane tube, m
R_2 = the radius of the reactor, m
L = the length of the reactor, m
R_g = gas constant, J mol^{-1} K^{-1}
T = temperature, K
$\tilde{v}_t$ = dimensionless linear velocity
ε = void fraction in PBR
ρ_{cat} = density of catalyst, g m^{-3}
δ_{mem} = membrane thickness, m
λ = characteristic PBMR length scale for multiple tubes, m

Literature Cited

1. Biloen P, Dautzenberg FM, Sachtler WMH. Catalytic dehydrogenation of propane to propene over platinum and platinum-gold alloys. *J Catal*. 1977;50(1):77–86.
2. Suzuki I, Kaneko Y. Dehydrogenation of propane over chromia-alumina potassium oxide catalyst. *J Catal*. 1977;47(2):239–248.

3. Derossi S, Ferraris G, Fremiotti S, Garrone E, Ghiotti G, Campa MC, Indovina V. Propane dehydrogenation on chromia silica and chromia alumina catalysts. *J Catal*. 1994;148(1):36–46.
4. Barias OA, Holmen A, Blekkan EA. Propane dehydrogenation over supported Pt and Pt-Sn catalysts: catalyst preparation, characterization, and activity measurements. *J Catal*. 1996;158(1):1–12.
5. Annaland TV, Kuipers JAM, van Swaaij WPM. A kinetic rate expression for the time-dependent coke formation rate during propane dehydrogenation over a platinum alumina monolithic catalyst. *Catal Today*. 2001;66(2–4):427–436.
6. van Miltenburg A, Zhu W, Kapteijn F, Moulijn JA. Adsorptive separation of light olefin/paraffin mixtures. *Chem Eng Res Des*. 2006; 84(A5):350–354.
7. Sirkar KK, Shanbhag PV, Kovvali AS. Membrane in a reactor: a functional perspective. *Ind Eng Chem Res*. 1999;38(10):3715–3737.
8. Coronas J, Santamaria J. State-of-the-art in zeolite membrane reactors. *Top Catal*. 2004;29(1–2):29–44.
9. McLeary EE, Jansen JC, Kapteijn F. Zeolite based films, membranes and membrane reactors: progress and prospects. *Microporous Mesoporous Mater*. 2006;90(1–3):198–220.
10. Ziaka ZD, Minet RG, Tsotsis TT. A high-temperature catalytic membrane reactor for propane dehydrogenation. *J Membr Sci*. 1993; 77(2–3):221–232.
11. Ziaka ZD, Minet RG, Tsotsis TT. Propane dehydrogenation in a packed-bed membrane reactor. *AIChE J*. 1993;39(3):526–529.
12. Collins JP, Schwartz RW, Sehgal R, Ward TL, Brinker CJ, Hagen GP, Udovich CA. Catalytic dehydrogenation of propane in hydrogen permselective membrane reactors. *Ind Eng Chem Res*. 1996;35(12): 4398–4405.
13. Kong CL, Lu JM, Yang HH, Wang JQ. Catalytic dehydrogenation of ethylbenzene to styrene in a zeolite silicalite-1 membrane reactor. *J Membr Sci*. 2007;306(1–2):29–35.
14. Kim SJ, Xu Z, Reddy GK, Smirniotis P, Dong JH. Effect of pressure on high-temperature water gas shift reaction in microporous zeolite membrane reactor. *Ind Eng Chem Res*. 2012;51(3):1364–1375.
15. Wu JCS, Liu PKT. Mathematical-analysis on catalytic dehydrogenation of ethylbenzene using ceramic membranes. *Ind Eng Chem Res*. 1992;31(1):322–327.
16. Kumar S, Gaba T, Kumar S. Simulation of catalytic dehydrogenation of cyclohexane in zeolite membrane reactor. *Int J Chem React Eng*. 2009;7:A13.
17. van den Bergh J, Gucuyener C, Gascon J, Kapteijn F. Isobutane dehydrogenation in a DD3R zeolite membrane reactor. *Chem Eng J*. 2011;166(1):368–377.
18. Harold MP, Lee C, Burggraaf AJ, Keizer K, Zaspalis VT, Delange RSA. Catalysis with inorganic membranes. *MRS Bull*. 1994;19(4): 34–39.
19. Gokhale YV, Noble RD, Falconer JL. Effects of reactant loss and membrane selectivity on a dehydrogenation reaction in a membrane-enclosed catalytic reactor. *J Membr Sci*. 1995;103(3):235–242.
20. Tsai CY, Ma YH, Moser WR, Dixon AG. Modeling and simulation of a nonisothermal catalytic membrane reactor. *Chem Eng Commun*. 1995;134:107–132.
21. Shelepova EV, Vedyagin AA, Noskov AS. Effect of catalytic combustion of hydrogen on the dehydrogenation processes in a membrane reactor. I. Mathematical model of the process. *Combust Explos Shock Waves*. 2011;47(5):499–507.
22. Gobina E, Hou K, Hughes R. Equilibrium-shift in alkane dehydrogenation using a high-temperature catalytic membrane reactor. *Catal Today*. 1995;25(3–4):365–370.
23. Casanave D, Ciavarella P, Fiaty K, Dalmon JA. Zeolite membrane reactor for isobutane dehydrogenation: experimental results and theoretical modelling. *Chem Eng Sci*. 1999;54(13–14):2807–2815.
24. Gallucci F, De Falco M, Tosti S, Marrelli L, Basile A. Co-current and counter-current configurations for ethanol steam reforming in a dense Pd-Ag membrane reactor. *Int J Hydrogen Energy*. 2008; 33(21):6165–6171.
25. Moon WS, Park SB. Design guide of a membrane for a membrane reactor in terms of permeability and selectivity. *J Membr Sci*. 2000; 170(1):43–51.
26. Rosenbrock HH. Some general implicit processes for numerical-solution of differential-equations. *Comput J*. 1963;6(4):329–330.
27. Li Q, Sui ZJ, Zhou XG, Chen D. Kinetics of propane dehydrogenation over Pt-Sn/Al(2)O(3) catalyst. *Appl Catal A Gen*. 2011;398(1–2):18–26.
28. Gascon J, Tellez C, Herguido J, Menendez M. Propane dehydrogenation over a Cr_2O_3/Al_2O_3 catalyst: transient kinetic modeling of propene and coke formation. *Appl Catal A Gen*. 2003;248(1–2):105–116.
29. Staudt-Bickel C, Koros WJ. Olefin/paraffin gas separations with 6FDA-based polyimide membranes. *J Membr Sci*. 2000;170(2):205–214.
30. Krol JJ, Boerrigter M, Koops GH. Polyimide hollow fiber gas separation membranes: preparation and the suppression of plasticization in propane/propylene environments. *J Membr Sci*. 2001;184(2):275–286.
31. Bai S, Sridhar S, Khan AA. Recovery of propylene from refinery off-gas using metal incorporated ethylcellulose membranes. *J Membr Sci*. 2000;174(1):67–79.
32. Kikuchi E. Palladium/ceramic membranes for selective hydrogen permeation and their application to membrane reactor. *Catal Today*. 1995;25(3–4):333–337.
33. Violante V, Drioli E, Basile A. Catalytic ceramic membrane reactor design for hydrogen separation from inert-gas via oxidation. *J Membr Sci*. 1995;104(1–2):11–17.
34. Prabhu AK, Oyama ST. Development of a hydrogen selective ceramic membrane and its application for the conversion of greenhouse gases. *Chem Lett*. 1999;28(3):213–214.
35. Stoitsas KA, Gotzias A, Kikkinides ES, Steriotis TA, Kanellopoulos NK, Stoukides M, Zaspalis VT. Porous ceramic membranes for propane-propylene separation via the pi-complexation mechanism: unsupported systems. *Microporous Mesoporous Mater*. 2005;78(2–3):235–243.
36. Tang Z, Kim SJ, Reddy GK, Dong JH, Smirniotis P. Modified zeolite membrane reactor for high temperature water gas shift reaction. *J Membr Sci*. 2010;354(1–2):114–122.
37. Zhang YT, Wu ZJ, Hong Z, Gu XH, Xu NP. Hydrogen-selective zeolite membrane reactor for low temperature water gas shift reaction. *Chem Eng J*. 2012;197:314–321.
38. Giannakopoulos IG, Nikolakis V. Separation of propylene/propane mixtures using faujasite-type zeolite membranes. *Ind Eng Chem Res*. 2005;44(1):226–230.
39. Granato MA, Jorge M, Vlugt TJH, Rodrigues AE. Diffusion of propane, propylene and isobutane in 13X zeolite by molecular dynamics. *Chem Eng Sci*. 2010;65(9):2656–2663.
40. Grande CA, Gascon J, Kapteijn F, Rodrigues AE. Propane/propylene separation with Li-exchanged zeolite 13X. *Chem Eng J*. 2010; 160(1):207–214.
41. Gutierrez-Sevillano JJ, Dubbeldam D, Rey F, Valencia S, Palomino M, Martin-Calvo A, Calero S. Analysis of the ITQ-12 zeolite performance in propane-propylene separations using a combination of experiments and molecular simulations. *J Phys Chem C*. 2010; 114(35):14907–14914.
42. Bakker WJW, vandenBroeke LJP, Kapteijn F, Moulijn JA. Temperature dependence of one-component permeation through a silicalite-1 membrane. *AIChE J*. 1997;43(9):2203–2214.
43. Dong JH, Lin YS, Liu W. Multicomponent hydrogen/hydrocarbon separation by MFI-type zeolite membranes. *AIChE J*. 2000;46(10): 1957–1966.
44. Kanezashi M, Lin YS. Gas permeation and diffusion characteristics of MFI-type zeolite membranes at high temperatures. *J Phys Chem C*. 2009;113(9):3767–3774.
45. Hong M, Li SG, Falconer JL, Noble RD. Hydrogen purification using a SAPO-34 membrane. *J Membr Sci*. 2008;307(2):277–283.
46. Kanezashi M, O'Brien-Abraham J, Lin YS, Suzuki K. Gas permeation through DDR-type zeolite membranes at high temperatures. *AIChE J*. 2008;54(6):1478–1486.
47. van den Bergh J, Tihaya A, Kapteijn F. High temperature permeation and separation characteristics of an all-silica DDR zeolite membrane. *Microporous Mesoporous Mater*. 2010;132(1–2):137–147.
48. Gascon J, Kapteijn F, Zornoza B, Sebastian V, Casado C, Coronas J. Practical approach to zeolitic membranes and coatings: state of the art, opportunities, barriers, and future perspectives. *Chem Mater*. 2012;24(15):2829–2844.
49. Kim WG, Nair S. Membranes from nanoporous 1D and 2D materials: a review of opportunities, developments, and challenges. *Chem Eng Sci*. 2013;104:908–924.

Manuscript received July 7, 2014, and revision received Nov. 3, 2014.